ACCEPT/REJECT CRITERIA FOR STRUCTURAL CERAMICS:

PART 4: A COMPUTER SIMULATION OF NONDESTRUCTIVE RELIABILITY IN CERAMICS

G. Meyer, K. Fertig and J. Richardson
Rockwell International Science Center
Thousand Oaks, California 91360

and

A. G. Evans
Materials Department
University of California
Berkeley, California 94720

ABSTRACT

A computer simulation of nondestructure failure prediction in silicon nitride containing silicon inclusions has been developed. The preliminary application of the simulation examines the results of an inspection that uses a single transducer in the pitch/catch mode. The limitations of the inspection method, especially when applied to nonspherical inclusions, are exposed by the simulation. Also, the expected influences of the signal-to-noise ratio and the inclusion size distribution on the failure and rejection probabilities emerge from the analysis in quantitative form.

INTRODUCTION

Ceramic components are subject to failure from inclusions introduced during the fabrication stage of manufacture. The specific influence of various inclusion types on fracture have been studied for hot-pressed silicon nitride,[1] indicating that silicon inclusions are particularly deleterious. The present study will thus use results for silicon inclusions in silicon nitride to illustrate the analysis of structural reliability using nondestructive inspection methods.

Recent studies of nondestructive defect characterization in ceramics have indicated that ultrasonic methods have the greatest potential for obtaining the information concerning defect size and type required for failure prediction.[2] One candidate technique with considerable promise is the combined use of low frequency ($\lesssim$0.5 ka, where k is the wave number and a is the defect radius) and high frequency ($\gtrsim$5 ka) scattering information. The high frequency scattering can be analyzed to provide information about the defect type;[3] while the low frequency results (given the defect type) can be analyzed to yield an estimate of the defect volume.[4,5] In the present study it is assumed that the defect type can be unambiguously determined (this has yet to be unequivocally demonstrated). Estimates of the defect volume, given that the defect is a silicon inclusion, can then be made using long wave length results. The analysis of reliability will thus be the optimum that can be achieved using the concept of combined high/low frequency scattering information. Methods for obtaining this information are described elsewhere.[6]

The probabilistic analysis yielding the parameters needed to reach accept/reject decisions, based on long wavelength ultrasonic scattering results, indicates false accept ψ_A and false reject ψ_R probabilities given by;[7]

$$\psi_A = \frac{\int_{-\infty}^{Y^*} \int_0^{\infty} \phi(Y|x)\ \Phi\ (S < \sigma_\infty|x)\ \phi(x)\ dY dx}{\int_0^{\infty} \Phi(S < \sigma_\infty)\ \phi(x)\ dx} \qquad (1)$$

$$\psi_R = \frac{\int_{0}^{Y^*} \int_0^{\infty} \phi(Y|x)\ \Phi\ (\sigma_\infty > S|x)\ \phi(x) dY dx}{\int_0^{\infty} \Phi\ (\sigma_\infty > S)\ \phi(x) dx}$$

The probability $\Phi(S < \sigma_\infty|x)$ that the strength S will be less than the applied stress σ_∞, given the inclusion dimensions x, is derived from an analysis of data obtained for fracture from silicon inclusions in silicon nitride.[1] The probability $\phi(Y|x)dY$ that the long wavelength estimate Y of the inclusion dimensions x are in the range Y to Y + dY is obtained from the analysis of scattering by spheroidal inclusions in the long wavelength limit.[5] The probability $\phi(x)dx$ - the a priori inclusion size distribution - is assumed to conform to an extreme value distribution, typical of defect distributions in ceramics.[8]

The objective of the present study is to obtain false-accept/false-reject probabilities pertinent to long wavelength scattering from silicon inclusions in silicon nitride. The inspection is confined to the conventional, single transducer pitch/catch configuration. Subsequent studies will examine other transducer configurations, in an attempt to identify optimum transducer arrays for minimizing the false-reject probability.

THE FUNDAMENTAL PROBABILITIES

The Inclusion Size

The inclusions are considered to be spheroidal, typical of the silicon inclusions observed in hot-pressed silicon nitride.[1] The state $\underline{x}$ adopted in the present study is the size and orientation of silicon inclusions in silicon nitride

$$\underline{x} = (\theta, \phi, \ell_1, \ell_2) \qquad (2)$$

where θ and ϕ are defined in Fig. 1, and ℓ_1 and ℓ_2 are the two semiaxis lengths of the spheroid.

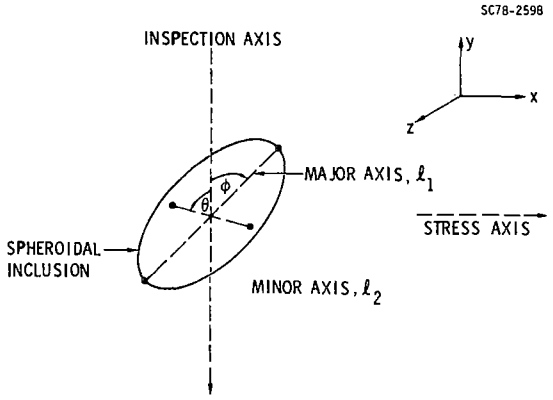

Fig. 1 A schematic indicating the orientation relationships for the spheroidal inclusions used in the simulation.

The angle ϕ is a uniform random variate on the interval $[0, 2\pi]$ and the direction cosine γ_z (= $\cos\theta$) is a Beta random variate with parameters ν_1 and ν_2. For the preliminary analysis $\nu_1 = \nu_2 = 1$, so that γ_z is a uniform random variate on the interval [0,1]. The lengths ℓ_1 and ℓ_2 of the semiaxis are assumed to be jointly distributed with density

$$P_{\ell_1, \ell_2}(x,y) = A\, f_{\ell_1}(x)\, f_{\ell_2}(y) L(\ell_2 - \ell_1) \qquad (3)$$

where

$$L(q) = \begin{cases} 0 & \text{if } q < 0 \\ 1 & \text{if } q \geq 0 \end{cases}$$

and A is chosen such that

$$\int_0^\infty \int_0^\infty P_{\ell_1, \ell_2}(x,y)\,dx\,dy = 1$$

The univariate densities are assumed to be extreme value and of the Weibull family, as often observed for the large extreme,[8]

$$f_{\ell_1}(x) = (x/b^*)^{k-1} \left(\frac{k}{b^*}\right) \exp\left(-x/b^*\right)^k \qquad (4a)$$

and

$$f_{\ell_2}(y) = (y/a^*)^{k-1} \left(\frac{k}{a^*}\right) \exp\left(-(y/a^*)^k\right) \qquad (4b)$$

where k is the shape parameter and a* and b* are the scale parameters. It can easily be shown that

$$A = 1 + \left(\frac{b^*}{a^*}\right)^k . \qquad (5)$$

To obtain Monte Carlo values for ℓ_1 and ℓ_2 a random variate was taken from each of the distributions

$$F_{\ell_1}(x) = 1 - \exp\left(-(x/b^*)^k\right)$$

and (6)

$$F_{\ell_2}(y) = 1 - \exp\left(-y/a^*\right)^K)$$

where k, a* and b* are input parameters. If $\ell_2 < \ell_1$, both random variates are discarded and two more are randomly selected. This is continued until two are selected such that $\ell_1 \leq \ell_2$ is far more likely than $\ell_2 < \ell_1$.

For the prediction of fracture it is required to obtain, from the state $\underline{x}$, the lengths of the semiaxes of the cross-sectional ellipse at the middle of the inclusion. If the stress is applied along the laboratory x-axis, the major axis a is simply

$$a = \ell_2;$$

while if $\xi = 1 - \gamma_x$ (γ_x is the direction cosine with respect to the x axis), the minor axis, b, can be obtained from

$$\frac{1}{b^2} = \frac{1}{\ell_2^2} + \left(\frac{1}{\ell_1^2} - \frac{1}{\ell_2^2}\right)\xi \quad . \qquad (7)$$

The Fracture Probability

The fracture model applied to the data for silicon inclusion initiated failure in silicon nitride has been derived[1] on the premise that the silicon inclusion fractures sub-critically to create a crack equal in size to the cross-sectional area of the inclusion. The predicted fracture stress σ_p can, for this model, be written as;

$$\sigma_p = Z(b/a) K_c b^{-1/2} \qquad (8)$$

where

$$Z(u) = \frac{1}{\sqrt{\pi}} \int_0^{\pi/2} (1 - (1 - u^2)\sin^2\theta)^{1/2}\, d\theta$$

and K_c is the fracture toughness of the silicon nitride matrix, assumed to be 5 MPa $\sqrt{m}$. Analysis of the fracture data indicated that σ_p was normally distributed, yielding a fracture probability at an applied stress σ_∞ given by;

$$\Phi(\sigma_\infty < S | \underline{x}) = B\left(\frac{\sigma_\infty - \alpha - \beta\sigma_p}{\sqrt{V(E_s)}}\right) \qquad (9)$$

where

$$B(x) = \frac{1}{\sqrt{2\pi}} \int_{-\infty}^{x} e^{-t^2/2}\, dt$$

E_s is a normal random variate describing the fracture strength S, with a variance $V(E_s)$ and a mean of zero; α and β are constants, given by;

$$\alpha = 99.66 \text{ MPa}, \quad \beta = 0.541 .$$

The location of the cross section of the inclusion at which inclusion fracture initiates has not yet been studied in detail. Presumably, the location will depend on the size distribution of pre-existing microcracks within the inclusion, or at the interface, and will exhibit some statistical variability. For the present analysis it is assumed that fracture occurs at the location with the maximum cross section exposed to the applied stress. This simplification eliminates one probability term from the final expression for the false-accept/reject probability; it also affords a lower limit for the fracture probability.

THE SCATTERING AMPLITUDE

The amplitude of a plane ultrasonic wave scattered in any direction by a spheroidal inclusion in the long wavelength limit can be calculated knowing the elastic properties of the inclusion and matrix as well as the axes and orientation of the spheroid.[4,5] This amplitude A is related to the frequency f by;

$$A = A_2 f^2 \tag{10}$$

where A_2 is a coefficient. The coefficient A_2 is used as a measure of the volume of the scatterer. The experimental determination of A_2 involves an error, associated both with background and extraneous reflections. It is assumed for the present calculation that the measured coefficient, Y (i.e., the slope of the amplitude in the f^2 scattering regime) is related to the absolute coefficient A_2 by;

$$(Y|\underline{x}) = A_2 + E_y \tag{11}$$

where E_y is a normal random variate with mean u = o and variance $V(E_y)$. The measured values† of the amplitude coefficient y thus have the conditional frequency distribution

$$h_{Y|\underline{x}}(y) = \frac{1}{\sqrt{V(E_y)}} \; H\left(\frac{y-A_2}{\sqrt{V(E_y)}}\right) \tag{12}$$

where,

$$H(y) = \frac{1}{\sqrt{2\pi}} \; e^{-y^2/2}$$

†Measured values of parameters are expressed in lower case, while the random variable from which the measurement is obtained is expressed in upper case.

THE FAILURE PROBABILITY

The intent of this section is to derive the probability of failure, given values for the measured ultrasonic scattering coefficient Y and the applied stress σ_∞.

If N is the number of Monte Carlo iterations, the estimate of the fracture probability is

$$\hat{\Phi}(S<\sigma_\infty) = \frac{1}{N} \sum_{i=1}^{N} B\left(\frac{\sigma_\infty - \alpha - \beta(\sigma_p)_i}{V(E_s)}\right), \tag{13}$$

and the estimate of the distribution of measured amplitude coefficients is

$$\hat{f}_y(y) \equiv F(Y) = \frac{1}{N} \sum_{i=1}^{N} \frac{1}{\sqrt{V(E_y)}} \; H\left(\frac{y-(A_2)_i}{\sqrt{V(E_y)}}\right). \tag{14}$$

Since the ultrasonic scattering and the fracture stress are stochastically independent in the present study, the estimate of the fracture probability for specific values of the ultrasonic amplitude coefficient becomes;

$$\hat{\Phi}(S<\sigma_\infty|Y) = \frac{\sum_{i=1}^{N} B\left(\frac{\sigma_\infty - \alpha - \beta(\sigma_p)_i}{\sqrt{V(E_s)}}\right) H\left(\frac{y-(A_2)_i}{\sqrt{V(E_y)}}\right)}{\sum_{i=1}^{N} \left(\frac{y-(A_2)_i}{\sqrt{V(E_y)}}\right)} \tag{15}$$

These three probabilities can be estimated by specifying values of the applied stress (σ_∞), the inclusion size parameters (a*, b* and k) and the measurement variance ($V(E_y)$), i.e., the signal-to-noise ratio. Preliminary results are obtained for a given applied stress of 250 MPa and three different values of the inclusion size and the measurement variance (Figs. 2(a), (b), (c)). Inspection of Fig. 2 indicates several important features. Firstly, note that the inclusion size distribution parameters have been chosen to enable the fracture probability without inspection $\Phi(S<\sigma_\infty)$ to be relatively invariant (ranging from 0.11 to 0.16). However, the location of the maximum density of scattering amplitudes F(Y) varies considerably. The trend toward a narrower distribution of Y from Fig. 2(a) to 2(c), reflects primarily the increase in the shape parameter k, with an additional superimposed influence of a decreasing signal-to-noise ratio. The most important results are the estimates of the variation in the fracture probability after ultrasonic inspection. This probability is just the probability of fracture at given values of the ultrasonic measurement amplitude Y, i.e., it is normalized by the distribution of Y values and contains no explicit dependence on this distribution. It would normally be anticipated that this probability should increase continuously as the measurement amplitude increases commencing, at small Y, below the fracture probability without

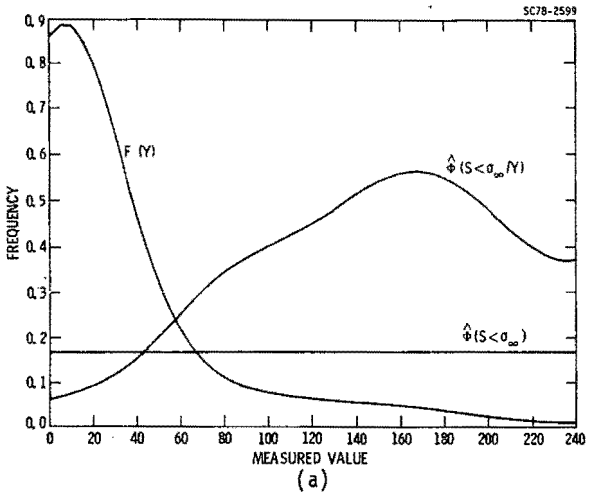

(a)

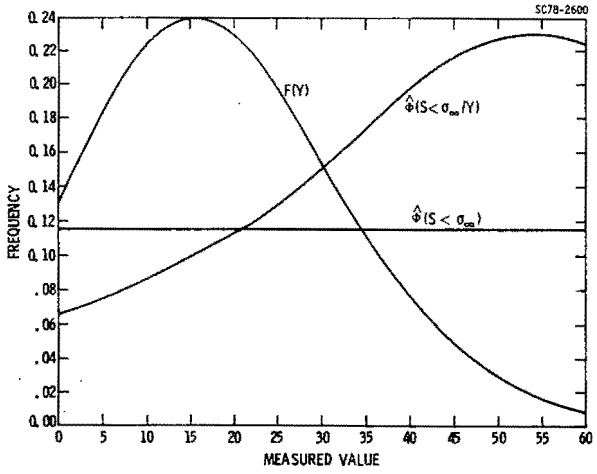

(b)

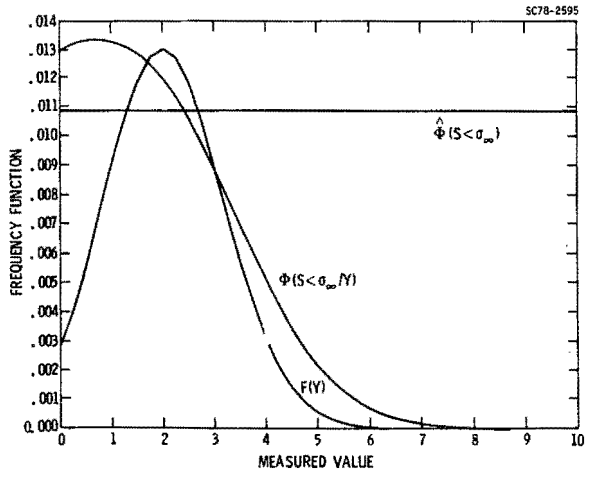

(c)

Fig. 2 Plots of the distribution of measured ultrasonic amplitudes F(V), the failure probability without inspection $\Phi(S<\sigma_\infty)$ and the failure probability corresponding to a speific ultrasonic indication $\Phi(S<\sigma_\infty/Y)$.

inspection. This behavior, referred to as "normal behavior", is observed for the parameters chosen to compute the failure probabilities reproduced in Figs. 2a and b. However, the inverse trend is observed in Fig. 2(c), referred to as "abnormal behavior". The rationale for this phenomenon involves the following considerations. The large k chosen for this calculation implies a narrow distribution of inclusion sizes, as reflected in the narrow range of F(Y) values in Fig. 2(c). This effect, coupled with the relatively large aspect ratio of the inclusions ($a^*/b^* = 10$), leads to the realization that the large extreme of F(Y) values refers to inclusions with their long dimension (a) nearly normal to the inspection direction. Yet, since the stress is applied normal to the inspection orientation, the cross section subject to fracture (for inclusions in this orientation) is small, $\approx b$. It can thus be concluded that inclusions which yield large scattering amplitudes can exhibit low fracture probabilities. The inspection in this instance is thus providing misleading information about failure, and could be deleterious to failure prediction, in the absence of ancilliary information. This effect will be minimized, and probably eliminated, by collecting scattering information at other angles. The benefits to be derived from inspection procedures other than the pitch/catch method will be the subject of a subsequent study.

FALSE ACCEPT/FALSE REJECT PROBABILITIES

The estimates of the false-accept and false-reject probabilities are derived from Eqn. (1); for example, the false-accept probability is given by;

$$\hat{\psi}_A\,(y|S<\sigma_\infty) = \frac{\sum_{i=1}^{N} B \left(\frac{\sigma_\infty - \alpha - \beta(\sigma_p)_i}{\sqrt{V(E_s)}}\right) H\left(\frac{y-(A_2)_i}{\sqrt{V(E_Y)}}\right)}{\sqrt{V(E_Y)} \sum_{i=1}^{N} B \left(\frac{\sigma_\infty - \alpha - \beta(\sigma_p)_i}{\sqrt{V(E_s)}}\right)} \quad (16)$$

The false-accept and false-reject probabilities derived for the three cases discussed in the preceding section are plotted in Fig. 3. The separation of the peak densities of these two distributions affords a measure of the reduced false-reject rate that can be achieved by inspection. The separation is most apparent in Fig. 3(b): a case in which the signal-to-noise ratio is not excessive and the inclusion aspect ratio (and size distribution) does not lead to "abnormal" behavior of the fracture probability after inspection. The much reduced separation for the case shown in Fig. 3(a) is primarily a consequence of the relatively large signal-to-noise ratio in this simulation, while the separation in case(c) reflects the aspect ratio problem discussed in the preceding section.

Additional simulations will be conducted in subsequent studies to examine independent effects of the signal-to-noise ratio, the inclusion aspect ratio and the inclusion size distribution.

It should be noted that although the false-accept/reject relations afford a unique relative measure of the utility of different inspection methods, two other probabilities are of greater

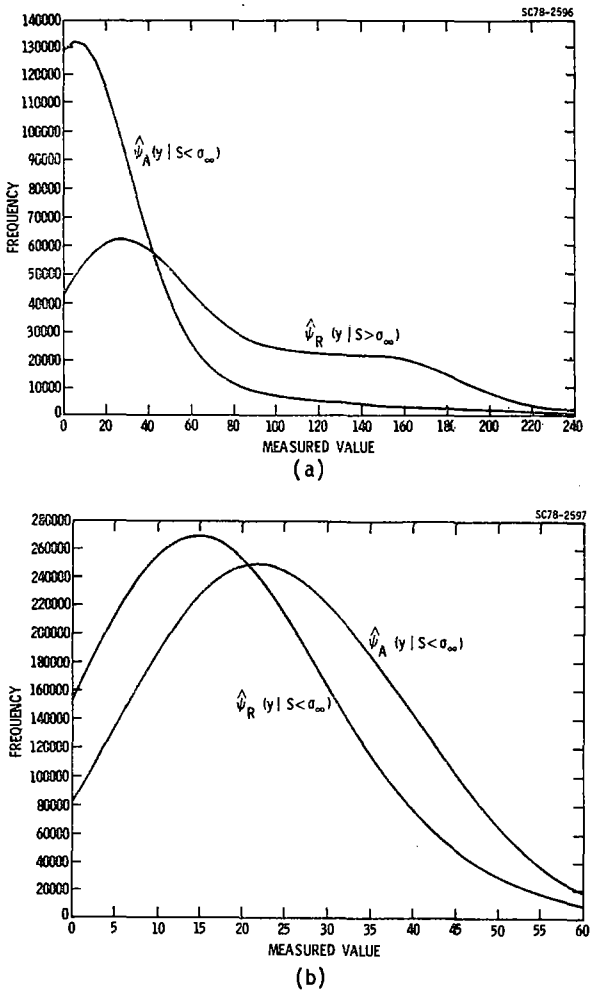

Fig. 3 Plots of the false-accept and false/reject probabilities as a function of the measure ment amplitude.

practical interest. The first is the probability of failure of components accepted by the inspection, i.e., the in-service failure probability P_F;

$$P_F(Y^*, \sigma_\infty) = \frac{\Phi(S < \sigma_\infty) \int_{-\infty}^{Y^*} \psi_A(Y|S<\sigma_\infty)dY}{\int_{-\infty}^{Y^*} F(Y)dY} \quad (17)$$

The other probability of interest is the total proportion of components rejected by the inspection, both falsely and correctly. This rejection probability P_R is simply

$$P_R = \int_{Y^*}^{\infty} F(Y)dY. \quad (18)$$

It may also be of interest to ascertain that proportion of the rejection probability attributed to false-rejection $(P_R)_F$;

$$(P_R)_F = \Phi(S<\sigma_\infty) \int_{Y^*}^{\infty} \psi_R (Y|S>\sigma_\infty)dY. \quad (19)$$

Each of these probabilities can be derived from the curves presented in Figs. 2 and 3.

ACKNOWLEDGEMENT

This research was sponsored by the Center for Advanced NDE, operated by the Science Center, Rockwell International, for the Defense Advanced Research Projects and the Air Force Materials Laboratory under Contract F33615-74-C-5180.

REFERENCES

1. A. G. Evans, B. I. Davis, G. Meyer and H. R. Baumgardner, to be published.
2. A. G. Evans, Naval Research Reviews, to be published.
3. Y. Murakami, B. T. Khuri-Yakub, G. S. Kino, J. R. Richardson and A. G. Evans, Jnl. Appl. Phys., to be published.
4. W. Kohn and J. R. Rice, Jnl. Appl. Phys. to be published.
5. J. R. Richardson, to be published.
6. R. K. Elsley and J. R. Richardson to be published.
7. J. R. Richardson and A. G. Evans, to be published.
8. A. G. Evans, L. Ahlberg, B. R. Tittmann, B. T. Khuri-Yakub and G. S. Kino, Jnl. Appl. Phys., 49 (1978) 2669.

Robb Thomson, Chairman (NBS): We have a few minutes for discussion. Tony hasn't used all of his hour. Are there any questions?

Paul Höller (Saarbrucken): I was astonished by the limit of detection you mentioned for micro-focus X-ray. What was the diameter of focus you were using and what was the focusing system?

Anthony G. Evans (Science Center): I am in an odd position here because John Schuldies did the experiment. Did you hear that question, John?

John Schuldies (Airesearch): I think I did. The size of the focal spot in that system theoretically approaches 50 microns depending on the bias applied to the electron beam prior to hitting the target. It is a commercially available system manufactured by Magnaflux.

Anthony G. Evans: Maybe I can ask you a question, Professor Holler. Was the purpose of the question that you know of a system which might be capable of detecting surface inclusions of a smaller size, or was it the other way around; you were impressed how small it was?

Paul Höller: I think there are instruments which have fine focus which will give better resolution. I suppose you are aware of the work which has been done in Harwell. Their instrumentation is commercially available, so we have preliminary results which are going much below the 250 microns you were mentioning here.

Anthony G. Evans: Again, I don't know quite how to respond to that since I am not personally involved in the X-rays. My feeling is that the focal spot, the resolution, is not a problem here. The biggest problem is that the difference in the X-ray absorption by the defect is not sufficiently different from that of the matrix. When you have appreciable thicknesses of the component, you really can't see anything. Maybe there are some further things to be done.

Joseph Matakey (TRW): I have two questions. The first is: Can you scan complex geometry with a high frequency ultrasonic technique; and the second one is: What is the low frequency range?

Anthony G. Evans: The answer to the first question is an interesting one and we have got some thoughts on that which I can describe. The low frequency, in this case, was 15 megahertz. It was a focused system. Bob Addison did that work and he will describe that in one of the posters this afternoon. It turns out we probably need somewhat higher frequencies than that in order to get the smallest defects of importance--perhaps, 35 megahertz. As far as the complex shape is concerned, we have a number of concepts that we have been working on with the use of buffers, that is, a ceramic which has one flat surface and the other surface contoured to fit the geometry of the component. Most of these components have to be machined very accurately any way to make sure they will satisfy the service requirements. One can, therefore, make a buffer for much of the component with great accuracy (within a mil or less) and then one can scan over the flat surface of the buffer and get through to the ceramic.

Joseph Matakey: Have you tried it?

Anthony G. Evans: We tried it. I say "we." Neil Kuriakin, at Stanford, tried it in the case of a sperical ceramic ball. We had a matching buffer with the flat surface and it worked very well. Part of this program is, now, to expand those concepts to ceramic turbine parts to see how well it works there. The signs look fairly good.

Daniel Isaac (ITT): When you mentioned that the bulk area of the void is significant, did you mean that for all states of stress, or did you refer to that portion of the area that is subject to tensile stresses?

Anthony G. Evans: That comes out in the integration. When you work out the integral, you integrate over that fraction of the area under tension. Since that is a constant fraction of the total area of the void (regardless of shape) and because it is a constant fraction, you can take the total area outside the integral.

Daniel Isaac: But the fraction depends on the state of stress. It is not a constant fraction.

Anthony G. Evans: It depends on the state of stress, certainly. I refer to the uniaxial case. For a biaxial or triaxial stress condition, you're absolutely right.

George Rudder (Ames Laboratory): Have you tried using different polarizations at high frequencies to distinguish the different types of voids?

Anthony G. Evans: The people at Stanford have developed transducers for longitudinal and shear waves. In the program we have also developed inverse response functions for both longitudinal and shear waves.

Jerry Tiemann (General Electric): In one of your earlier slides you showed the fracture response as a function of the thickness of the void for silicon, tungsten carbide and other ionic types. One would have thought that they would have converged to the same level at zero thickness, but in fact, all the curves seem to approach different intercept values. Would you comment on the origin of that variance?

Anthony G. Evans: Let me see if I can find it so I can point out to everybody what you mean. You see I didn't take them to zero. The reason for that, of course, is that, if the defect thickness is really zero, the strength goes to the theoretical strength. So all of these curves should go to the theoretical strength at zero thickness. I referred to measurements that we actually made. The smallest defect we had in there was 50 microns. The actual results have to go up very, very rapidly to yield theoretical strengths at zero thickness.

Robb Thomson, Chairman: I think one more question, then.

Thomas De Lacy (Ford Aerospace): I am surprised that you continue to look at single discrete defects. Why aren't we looking at the effects of the interrelation of size distribution and maybe a range of inclusions or particulates within the material?

Anthony G. Evans: The reason that we have confined ourselves to so-called isolated defects, not interacting defects, is that our initial interest is in the case of a hot pressed silicon nitride for which all our fracture studies have indicated that (except in rare cases) fracture does indeed occur from individual, isolated inclusions or from surface cracks. There are no interaction effects between them. That's not the case, I know, in reaction bonded silicon nitride where, clearly, one has interaction effects before fracture.

Thomas De Lacy: But, you know, there are regression and oxidation mechanisms. There are lots of things that could be interrelated to the behavior of the ceramic in service; but your whole study is ceramic fracture. I guess that's the key.

Anthony G. Evans: There is a lot of work going on in the program in that vein in recognizing that oxidation does introduce a new population of surface cracks that weren't there at the onset of the inspection. What we find out, though, is that that population tends to level off after a certain while. There is a plateau in the strength as a function of oxidation time as it turns out. To design below that level, then, one is concerned with the cracks that existed prior to the oxidation which are deeper than the oxidation layer. That is our present prospective.

Thomas De Lacy: I understand, but the mechanism that might be working is the synergistic effect. Improved understanding of the oxidation mechanism that could change the chemical bond state is rather interesting. We looked at that some time ago at General Dynamics. I was associated with Mossbauer spectroscopy and there are lots of techniques that could be interrelated to this kind of work that could be very valuable. I am surprised we are not doing some of that.

Anthony G. Evans: I think your surprise will be moderated when you start looking at the dollars that will be mounted up even for the number of tests we have conducted. It is a lot of dollars. You are right, though. I think one should always have in the back of one's mind that these effects are occurring in service and they do modify the roughness of it as well as the flaw size. I think that is going to be further down the road.

Robb Thomson, Chairman: I think at this point we should terminate this part and go on to the next lecture.